

Stochastic Simulation of DNA Double-Strand Break Repair by Non-homologous End Joining Based on Track Structure Calculations

Author(s): Werner Friedland, Peter Jacob, and Pavel Kunderát

Source: Radiation Research, 173(5):677-688.

Published By: Radiation Research Society

DOI: <http://dx.doi.org/10.1667/RR1965.1>

URL: <http://www.bioone.org/doi/full/10.1667/RR1965.1>

BioOne (www.bioone.org) is a nonprofit, online aggregation of core research in the biological, ecological, and environmental sciences. BioOne provides a sustainable online platform for over 170 journals and books published by nonprofit societies, associations, museums, institutions, and presses.

Your use of this PDF, the BioOne Web site, and all posted and associated content indicates your acceptance of BioOne's Terms of Use, available at www.bioone.org/page/terms_of_use.

Usage of BioOne content is strictly limited to personal, educational, and non-commercial use. Commercial inquiries or rights and permissions requests should be directed to the individual publisher as copyright holder.

Stochastic Simulation of DNA Double-Strand Break Repair by Non-homologous End Joining Based on Track Structure Calculations

Werner Friedland,¹ Peter Jacob and Pavel Kunderát

Helmholtz Zentrum München, Institute of Radiation Protection, 85764 Neuherberg, Germany

Friedland, W., Jacob, P. and Kunderát, P. Stochastic Simulation of DNA Double-Strand Break Repair by Non-homologous End Joining Based on Track Structure Calculations. *Radiat. Res.* 173, 677–688 (2010).

A Monte Carlo simulation model for DNA repair via the non-homologous end-joining pathway has been developed. Initial DNA damage calculated by the Monte Carlo track structure code PARTRAC provides starting conditions concerning spatial distribution of double-strand breaks (DSBs) and characterization of lesion complexity. DNA termini undergo attachment and dissociation of repair enzymes described in stochastic first-order kinetics as well as step-by-step diffusive motion considering nuclear attachment sites. Pairs of DNA termini with attached DNA-PK enter synapsis under spatial proximity conditions. After synapsis, a single rate-limiting step is assumed for clean DNA ends, and step-by-step removal of nearby base lesions and strand breaks is considered for dirty DNA ends. Four simple model scenarios reflecting different hypotheses on the origin of the slow phase of DSB repair have been set up. Parameters for the presynaptic phase have been derived from experimental data for Ku70/Ku80 and DNA-PK association and dissociation kinetics. Time constants for the post-synaptic phase have been adapted to experimental DSB rejoining kinetics for human fibroblasts after ¹³⁷Cs γ irradiation. In addition to DSB rejoining kinetics, the yields of residual DSBs, incorrectly rejoined DSBs, and chromosomal aberrations have been determined as a function of dose and compared with experimental data. Three of the model scenarios obviously overestimate residual DSBs after long-term repair after low-dose irradiation, whereas misrejoined DSBs and chromosomal aberrations are in surprisingly good agreement with measurements. © 2010 by Radiation Research Society

INTRODUCTION

Cells have evolved several pathways for repairing DNA double-strand breaks (DSBs) to maintain genome integrity. Non-homologous end joining (NHEJ) is the dominant DSB repair pathway in cells of multicellular eukaryotes during the G₁ phase of the cell cycle. The

NHEJ pathway has been investigated comprehensively, and various review articles (1–4) comprise essentials and refer to experimental findings on many steps within this process.

On the other hand, a variety of numerical models dealing with DSB repair processes have been developed and applied to experimental results, focused on various issues like the relationship between repair kinetics and cell survival (5, 6), induction of chromosomal aberrations (7, 8), formation of micronuclei (9), DNA fragmentation patterns (10), and influence of DNA damage complexity (11). Recently, a biochemical approach by modeling molecular events associated with NHEJ has been presented, aimed at simulating repair of DSBs produced by low-LET radiation (12). The induction of DSBs and activation pathways for major NHEJ components including Ku70/Ku80, DNA-PKcs and the ligase IV/XRCC4 heterodimer were described by a system of coupled non-linear ordinary differential equations. Induction of γ -H2AX foci after DNA-PKcs auto-phosphorylation was also modeled. The model faithfully reproduced several experimental end points including DSB rejoining at 10 min postirradiation or longer and the time course of γ -H2AX focus yields. However, the spatial dimension of the repair process was not considered in the model. Thus misrepair leading to mutation and chromosomal aberrations could not be addressed, and relationships between radiation quality and DSB complexity and the spatial dependence of initial DSBs could not be assessed.

The present simulation model is a first step toward a mechanistic description of important processes occurring in cells in response to a radiation insult in the time frame from milliseconds up to days; thus it extends by about 13 orders of magnitude the temporal dimension of biophysical simulation calculations in the Monte Carlo code PARTRAC (13, 14), which effectively ends after a few 10 ns when no further OH radicals are active. The present work is focused on the simulation methodology and its application to a single experimentally investigated system. Data on the spatio-temporal distribution of DSBs and their complexity in terms of nearby DNA

¹ Address for correspondence: Helmholtz Zentrum München, Institute of Radiation Protection: Ingolstädter Landstr. 1, 85764 Neuherberg, Germany; e-mail: Friedland@helmholtz-muenchen.de.

lesions constitute the starting conditions of the calculation. This information is determined in PARTRAC by combining track structure calculations with sophisticated target models of the genomic DNA inside a mammalian cell nucleus. Repair enzyme activation and association at and dissociation from DNA termini are modeled in first-order kinetics by Monte Carlo method, complemented with step-by-step Brownian motion of DNA termini. Four simplistic hypothetical scenarios on the origin of the slow repair phase have been set up, adapted to experimental rejoining data, and analyzed regarding the end points of residual DSBs, misrejoined DSBs and induced chromosomal aberrations. Comparison with experimental results for similar irradiation systems allows basic testing of the assumptions underlying the model scenarios.

MATERIALS AND METHODS

Simulation of Initial DNA Damage

1. Track structure calculation

The biophysical Monte Carlo simulation code PARTRAC has been used to calculate the transport and energy deposition patterns of photons and secondary electrons. For photon interactions, the elemental composition of cell nuclei is considered and cross sections from ref. (15) have been adopted. For electrons, liquid water is taken as substitute for cells and cell nuclei; inelastic interaction cross sections are based on the work of Dingfelder *et al.* (16, 17). For the simulation of radiation chemistry processes in water surrounding the DNA in the cell nucleus, a recently updated parameter set has been used (18).

2. DNA target model

The DNA target model used in this investigation is based on a spherical chromatin domain (SCD) model of chromosomes of a human fibroblast cell in G₁ phase (19), integrated into PARTRAC (13). A human fibroblast cell nucleus is represented as an ellipsoid with axis lengths of 20 μm, 10 μm and 5 μm. The chromatin fiber in a cell nucleus comprises 1,214,000 cubic volume elements of 50 nm side length with a total genomic length of 6.6×10^9 bp. Chromatin fiber loops about 100,000 bp long are modeled by successive cubic elements periodically departing from and reapproaching the SCD centers; each local minimum in the distance from the SCD center acts as a nuclear attachment site at the basis of the chromatin fiber loop.

3. Calculation of single- and double-strand break induction

Single- and double-strand breaks in the DNA are calculated from superposition of calculated tracks onto the DNA target model, i.e., from energy deposition events inside the molecular volume of the sugar-phosphate backbone and from interactions of diffusing OH radicals with sugar moieties. Details on the calculation method are given in ref. (14).

For the calculation of absolute DSB yields, selected parameters have been adapted to align calculations with experimental results on DSB yields after ¹³⁷Cs γ irradiation of human skin fibroblasts (20). Good agreement has been obtained with the parameter set used in ref. (21) after ascribing half of the OH-sugar interactions leading to strand breaks to the production of heat-labile sites and the other half to strand breaks also occurring in cold lysis protocols. Thus DNA strand breaks from direct effects, i.e., energy depositions at or near atoms of the DNA backbone, occur with a probability that increases

linearly from 0 at 5 eV to 1 at 57.6 eV deposited energy, and from indirect effects, i.e., OH[•] attack, in 65% and 32.5% of OH[•]-sugar interactions after warm and cold lysis, respectively. Further assumptions on DSB induction have been adopted as in earlier investigations using PARTRAC (14, 22). Experimentally, 27.6 and 38.2 DSBs per cell and Gy have been reported after 40 Gy ¹³⁷Cs γ irradiation using cold and warm lysis protocols, respectively (20); the calculated DSB yields were 27.8 and 41.0 DSBs without and including heat-labile sites, respectively.

4. Calculation of base lesions

Base lesions from direct effects are scored in PARTRAC from superposition of energy deposition events with the volume of the union of atoms within the bases of the DNA with van der Waals radii multiplied by a factor of 2. Base lesions from indirect effects result from interactions of OH[•] with bases; interaction distances are given in ref. (22). It is assumed that only a certain fraction of the energy deposition and OH[•] interaction events lead to base lesions that have an influence on DNA repair kinetics. The probability for such relevant base lesions due to direct effects increases linearly from 0 at 0 eV deposited energy to 1 at 60 eV (and more) deposited energy and is 50% of all OH[•]-base interactions for lesions from indirect effects. No further classification of these relevant base lesions is made.

Simulation of DNA Repair via NHEJ

1. Clean and dirty DNA ends and initial condition

The principal items in the simulation of DNA repair are the 5' and the 3' termini of a broken DNA strand. DNA termini carrying nearby single-strand breaks and/or relevant base lesions are called dirty DNA ends, whereas clean DNA ends are DNA termini without such lesions; these nearby lesions are scored up to a sequence of 20 undamaged base pairs, corresponding to the damage cluster definition in ref. (22). Thus complex DSBs according to the usual notation (23) may include two dirty DNA ends or one dirty and one clean DNA end; a simple DSB comprises two clean DNA ends. Another DSB close to a DNA end without further damage is not taken as a dirty DNA end, but it generates a rather short fragment. DNA fragments of less than 25 bp are assumed to be not joinable since they are too short for the assembly of repair enzymes. It is noteworthy that such short DNA fragments generally are not detected in experiments and thus contribute to neither rejoining kinetics nor measured fractions of residual DSBs. With the assumptions above, the calculated 1114 DSBs (2228 DNA ends) produced by 40 Gy ¹³⁷Cs γ irradiation of human skin fibroblasts include 1401 clean DNA ends and 827 DNA dirty DNA ends; 6 DNA ends confine unrejoinable short DNA fragments.

The following attributes of DNA termini calculated by PARTRAC have been used as input data for the repair simulation:

- geometric position within the cell nucleus,
- genomic location on the chromosome,
- genomic length of the chromatin fiber between DSBs and the nearest attachment site at a nuclear matrix or, if shorter, length of the DNA fragment,
- adjacent single-strand breaks and relevant base lesions up to a sequence of 20 undamaged base pairs,
- information on the complementary DNA end, the other end of the produced fragments and the initiating primary particle,
- length of single-stranded overhang, used for supplementary calculations only.

2. Temporal development of DNA ends

The progress of DNA repair through a sequence of states is calculated as a stochastic process with first-order kinetics. Each

change of state of a DNA end is determined by a single parameter representing the time constant τ of the process: the probability for changing within time step δt is $1 - \exp(-\delta t/\tau)$; a time step of 0.01 s has been adopted in all calculations. In the present version of the model, time constants are spatially and temporally constant. Differently modeled is the conjunction of two DNA ends in a synaptic complex where interaction distance and probability parameterize the immediate parallel change of their states. After synapsis, changes in the state of one DNA end in the synaptic complex may cause instant changes in the state of the other DNA end, too. To describe the recovery of fluorescence after photobleaching (FRAP), DNA ends may change their states unconditionally at predefined times after the simulation begins. The final states of joined DNA ends are classified into correct rejoining, incorrect joining within the same chromosome, formation of rings (joining with the other end of the DNA fragment), and exchange chromosome aberrations.

3. Movement of DNA ends

Individual mobility of DNA termini is an essential issue for incorrect joining of DNA ends, in particular for the induction of chromosomal aberrations. Movement of DNA ends is represented in the simulation model as a step-by-step dislocation corresponding to stochastic Brownian motion in a homogeneous liquid; thus, apart from nuclear attachment sites (see below), no structures or characteristics of the DNA target model are taken into account in the calculation. DNA ends move under the spatial boundary conditions that (1) they remain within the cell nucleus, (2) pairs of DNA ends in synapsis do not move relative to each other, (3) ends of a short DNA fragment cut out of a chromatin loop stay in proximity, and (4) other DNA ends are confined to a sphere around the nearest nuclear attachment site at the base of the broken chromatin fiber loop; in this case, the radius is related to the chromatin fiber length between the DNA end and the attachment site and may increase linearly with time, reflecting gradual decondensation of the chromatin fiber. In the present calculations, a radius of 70 nm for up to 200 bp, increasing by 5 nm per additional 1000-bp chromatin fiber length, has been adopted that increases with time by 0.01 nm/s; for short fragments, the same dependence on genomic length is used for the maximum distance of the DNA ends.

Motion of DNA ends is parameterized by a diffusion coefficient D ; for each time step δt , the mean displacement is $\delta r = (6D\delta t)^{1/2}$. The diffusion coefficient adopted for DNA ends depends on their state, and, for short DNA fragments, on DNA fragment size. In the present work only a binary categorization of DNA ends has been made into states with low mobility, with a diffusion coefficient of $1 \text{ nm}^2/\text{s}$, or states with high mobility, with a diffusion coefficient of $100 \text{ nm}^2/\text{s}$. The higher value corresponds to the fast confined movement observed in live cell microscopy of damaged chromatin within minutes after irradiation with jump steps of about 75 nm within 10 s (24). Both diffusion coefficients are used for DNA ends of long DNA fragments, whereas short DNA fragments are assumed to have an enhanced diffusion coefficient with a functional dependence on DNA fragment size L according to $L^{-0.72}$ adopted from ref. (25). In view of corresponding mobility data for the cytoplasm and nucleus (25), the increased mobility has been restricted to termini of DNA fragments shorter than 2000 bp with a continuous progression to the constant values for DNA ends of larger fragments.

4. General scheme of the NHEJ process

The principal scheme of the model for DNA repair via non-homologous end joining is presented in Fig. 1. Within this general scheme, several scenarios have been setup and analyzed (see below). The repair process is divided into a presynaptic and a postsynaptic phase; important differences between the two phases are listed in Table 1.

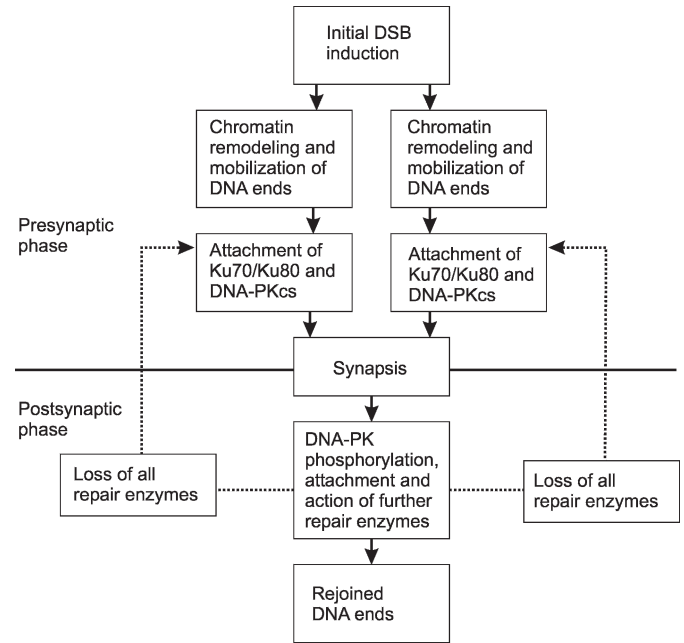


FIG. 1. Scheme of DNA repair model via NHEJ.

The presynaptic phase starts immediately after the production of radiation-induced DSBs with chromatin remodeling and mobilization of the two DNA ends (26). Then the two constituents of DNA-PK, the Ku70/Ku80 heterodimer and the catalytic subunit DNA-PKcs, bind sequentially to both DNA ends. Under given proximity conditions, two DNA ends with attached DNA-PK form a synaptic complex and enter the postsynaptic phase. In this phase, all further steps of the NHEJ pathway take place and states of DNA ends are interrelated. In one of the scenarios tested, possible failure of the repair process after synapsis is considered by assuming that synapsis is lost, all attached repair enzymes are dissociated, and the whole process restarts with Ku70/Ku80 attachment. At the end of the repair process, DNA ends are joined in the sense that the usual protocols of DSB induction and rejoining experiments no longer detect separate DNA fragments. The calculated fractions of DNA ends in rejoined states are compared with the measured fractions of rejoined DSBs irrespective of DNA fragment sizes and their detectability in the experimental protocol.

5. Modeling of the presynaptic phase of DNA repair via NHEJ

The presynaptic phase of the simulated DNA repair process is presented in Fig. 2. It comprises mobilization of DNA ends, attachment of Ku70/Ku80 with a concurrent blocking of Ku70/Ku80 attachment for mobilized DNA ends, and attachment of DNA-PKcs, and it ends with synapsis of two DNA ends with attached DNA-PK in proximity. The process of blocking Ku70/Ku80 attachment may reflect attachment of other species or geometrical constraints. Inverse dissociation processes are considered for Ku70/Ku80 attachment and its blocking; after attachment of DNA-PKcs it is assumed that the total DNA-PK complex may dissociate from DNA ends before synapsis with another DNA end has occurred. Two DNA ends with closely attached DNA-PKcs have a certain probability per simulation time step of forming a synaptic complex and entering the postsynaptic phase of the process.

Measurements of the association of Ku80 tagged with yellow fluorescence protein (YFP) with laser-induced DSBs showed an increase in the fluorescence signal with an initial time constant of about 5 s (27). The attachment of fluorescent DNA-PKcs was reported to have the same recruitment kinetics as Ku80 (27); however,

TABLE 1
Characteristics of the Two Phases of the NHEJ Process in the DNA Repair Model

Presynaptic phase	Postsynaptic phase
DNA ends are independent items	DNA ends are pairwise linked items
DNA ends have high mobility with respect to each other after initial mobilization and chromatin remodeling; experimental data on motion are scarce	DNA ends are immobile with respect to each other; much experimental data on common motion is available
Sequence of steps is supposed to be clear	Sequence of steps is not clear; they may occur in parallel
Kinetic data on association and dissociation of involved repair proteins are available	Kinetic data on involved repair proteins are missing
Steps are and kinetics may be independent of lesion complexity at DNA ends	Steps and kinetics depend on lesion complexity at DNA ends
Parameter determination is essentially based on kinetic data for individual repair proteins	Parameter determination is essentially based on kinetics of DNA repair after irradiation

in the corresponding figure an initial delay for DNA-PKcs of about 1 s is visible (see also Fig. 4 in this work). These experimental findings have been used to determine some time constants for our model (see Table 2 and Results). Measured dissociation rates of Ku70/Ku80 from DNA ends yielding a median value of $2 \times 10^{-3} \text{ s}^{-1}$ (28) are incorporated in the model by a time constant of 500 s for this process. For dissociation of DNA-PK from DNA ends, rates of $4.8 \times 10^{-2} \text{ s}^{-1}$ for 18-bp pieces of DNA and of $5 \times 10^{-3} \text{ s}^{-1}$ for >26-bp pieces of DNA, corresponding to time constants of 21 s and 200 s, respectively, have been reported (29). In the calculations, a time constant of 60 s has been used; with this value the time course of experimental data on fluorescence recovery after photobleaching of DNA-PKcs (27, 30) could be reproduced quite well in a dedicated repair model setup that distinguishes between fluorescent and photobleached states and mimics photobleaching 600 s after the repair process begins.

6. Modeling of synapsis and the postsynaptic phase of DNA repair via NHEJ

In the model, two DNA ends with attached DNA-PK undergo synapsis with a probability of 0.9 within the adopted time step of 0.01 s if they are not more than 20 nm apart; this interaction distance

reflects the size of a DNA-PK complex at DNA ends (31). The interaction probability has been chosen as an arbitrary high value to initiate this process typically whenever two such DNA ends encounter each other during diffusive motion.

The steps in the postsynaptic phase of the NHEJ model are presented in Fig. 3 for a pair comprising a clean and a dirty DNA end. For two clean DNA ends, the upper part of the figure has to be repeated in the lower part, whereas for two dirty DNA ends the upper part has to be replaced by the lower part in the figure. After synapsis, autophosphorylation of DNA-PK occurs and the NHEJ DNA repair pathway proceeds via attachment and activity of the XRCC4/ligase IV complex under promotion of XLF/Cernunnos (32). Due to the lack of time constants for individual repair enzymes, the postsynaptic phase has been set up for a pair of clean DNA ends by a single rate-limiting step for the attachment and activity of all further repair enzymes, following an arbitrary short autophosphorylation step with a time constant of 1 s. As soon as one of the two linked DNA ends has finished this step, final joining is assumed, provided that the other DNA end is clean. The time constant of this rate-limiting step has been determined from adaptation to experimental data (see Results). For dirty DNA ends, it has been assumed that nearby lesions have to be processed before final joining may occur. This cleaning process is

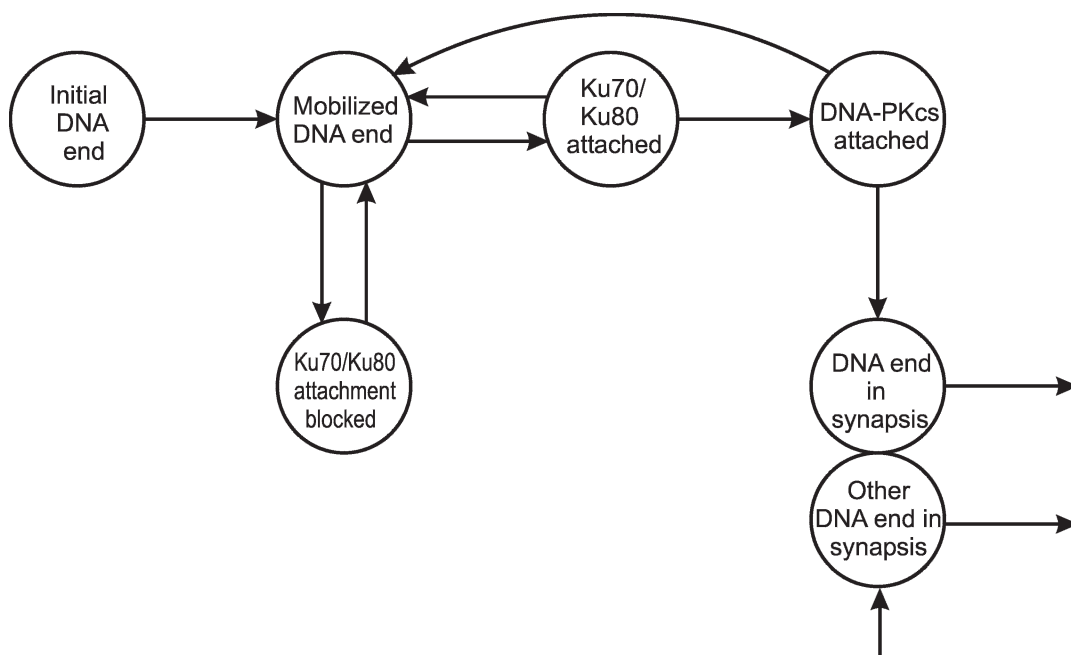


FIG. 2. Modeling of the presynaptic phase of DNA repair via NHEJ.

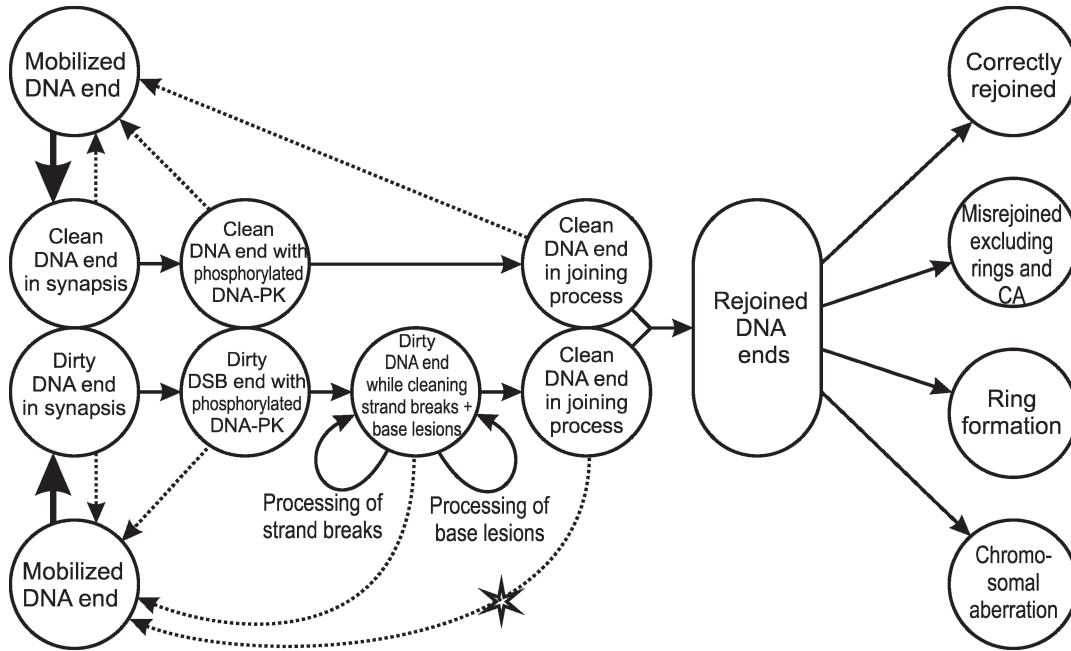


FIG. 3. Modeling of the postsynaptic phase of DNA repair via NHEJ for a pair of a clean and a dirty DNA end. Thick arrows represent the presynaptic phase; dotted arrows show the optional break-up of the synaptic state with complete loss of attached repair enzymes. The process marked with * involves a former dirty DNA end that has been cleaned and maintains this state during further processes.

considered as a step-by-step process for each relevant base lesion and each single-strand break close to the DNA end. After processing of all nearby lesions of a dirty DNA end, it is assumed that the end behaves like a clean DNA end, and the final joining step is modeled as for native clean DNA ends.

In one of the scenarios it has been assumed that even after synapsis the repair process may fail for all combinations of DNA ends. In that case, the synaptic complex is broken, all repair enzymes attached at both involved DNA ends are dissociated and the repair process is restarted with two independent DNA ends before Ku70/Ku80 attachment. If this dissociation occurs during the cleaning stage of dirty DNA ends, then the subsequent calculation restarts with an

accordingly reduced number of strand breaks and relevant base lesions as given by the cleaning steps that are already finished.

Time constants for the postsynaptic phase of NHEJ have been adapted to experimental DSB rejoining data for human fibroblast cells after irradiation with 40 Gy ¹³⁷Cs γ rays (20) after cold DNA extraction. These data show the usual biphasic behavior with a half-time of 7.5 min for the fast-repairing fraction of 48% and 2.7 h for the slowly repairing fraction. Because these experimental data (20) include a repair period of about 4 h, no information about the unrejoined fraction can be extracted after about 1 day. Simulation calculations for the four scenarios below have been adapted in particular regarding the initial repair rate within the first 20 min and the fraction of residual DSBs and their reduction in the phase of slower repair about 2 to 4 h after DSB induction. This adaptation has been aimed at achieving reasonable agreement but not at identification of a parameter set with minimum deviations.

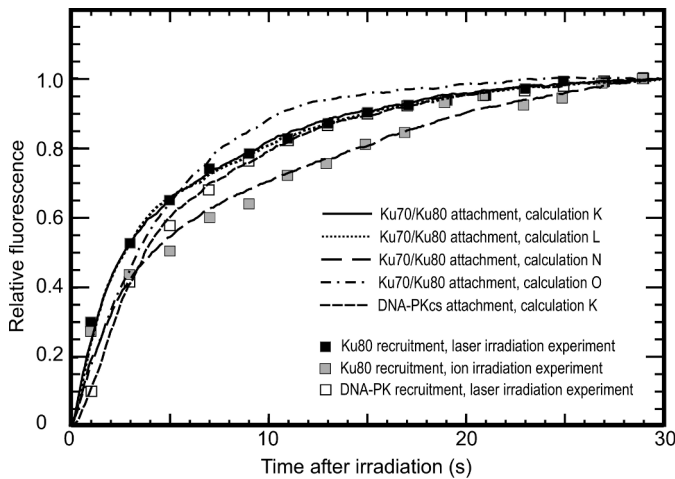


FIG. 4. Experimental data (27) for Ku80 recruitment after laser and ion irradiation and for DNA-PK recruitment after laser irradiation compared to model calculations with various parameter sets (see Table 2).

7. Scenarios for DNA repair calculations

The basic assumptions of four simple scenarios for DNA repair calculations are presented in Table 3. The time constants for the postsynaptic phase in the last two rows, obtained from parameter adaptation to experimental data (20), are discussed in the Results section.

In scenario A, diffusive motion of DNA ends is low throughout the repair process. As a consequence, formerly linked DNA ends remain predominantly in sufficient proximity during the presynaptic phase to undergo synapsis quite soon. According to scenario B, diffusive motion of DNA ends is permanently high after initial mobilization and results in frequent failure of early synapsis. In contrast, synaptic and subsequent repair processes are maintained at later times due to the frequent encountering of diffusing DNA ends. In scenario C, differences in the dynamics of clean and dirty DNA ends occur during the presynaptic phase; in particular, blocking of Ku70/Ku80 attachment occurs only for dirty DNA ends, which thus enter fast synapsis with a lower probability than pairs of clean DNA ends. Scenario D assumes that the repair process fails after synapsis for a

TABLE 2
Transfer Parameters for Model Calculations of the Presynaptic Phase

Process	Time constant (s)				
	K	L	M	N	O
Chromatin remodeling and mobilization of free DNA ends	1.5	0.1	0.1	1.5	0.1
Blocking of Ku70/Ku80 attachment to free DNA ends	0.3	3	0.2 ^a	0.15	— ^b
Release from Ku70/Ku80 blocking to DNA ends	5	4	3 ^a	5	— ^b
Attachment of Ku70/Ku80	0.3	4	3	0.3	5
Dissociation of DNA - Ku70/Ku80	500	500	500	500	500
Attachment of DNA-PKcs	1	1	1	1	1
Dissociation of DNA-PK	60	60	60	60	60

^a For dirty DNA ends.

^b Not defined for all DNA ends.

^c Not defined for clean DNA ends.

significant fraction of DNA ends. To combine a high fraction of DNA ends entering early synapsis with ongoing repair activity in later phases, it is assumed that an initially low diffusive motion in the presynaptic phase is increased after re-entering the initial state after dissociation of attached repair enzymes.

The calculations of DNA repair kinetics were based on the initial DNA damage of human fibroblasts after irradiation with 40 Gy ¹³⁷Cs γ rays (20). For comparisons with experimental results on misrejoined fractions, calculations for 80 Gy have been done. For the determination of dose-dependent yields of residual and misrejoined DSBs as well as chromosomal aberrations, DNA repair kinetics has been analyzed after irradiation with lower doses down to 1 Gy.

RESULTS

Parameter Adaptation for the Presynaptic Phase of DNA Repair

In Fig. 4, experimental data (27) on the attachment of Ku80 and DNA-PKcs after laser irradiation and of Ku80 after ion irradiation are presented in comparison to model calculations after parameter adaptation; the resulting time constants for the transfer processes are listed in Table 2. Good agreement between measured recruitment of Ku80 after laser irradiation and calculated Ku70/Ku80 attachment was obtained with parameters reflecting both calculation K (solid line) and calculation L (dotted line); similar kinetics was found for calculation M (not shown). Thus the time constants for the individual steps in the presynaptic phase cannot be identified unequivocally from such measurements. A time constant of 1 s for DNA-PKcs attachment reproduces the shift in the initial rise compared to Ku70/Ku80 (short-dashed line). Without consideration of blocking of Ku70/Ku80 attachment, the resulting recruitment curve for Ku70/Ku80, as in calculation O (dash-dot line), does not reproduce the reduction in the measured attachment rate after some seconds. Overall agreement with measured data on Ku80 recruitment after ion irradiation is obtained with a reduced time

constant of 0.15 s for blocking of Ku70/Ku80 attachment in calculation N (long-dashed line).

Parameter Adaptation for the Postsynaptic Phase of DNA Repair

In Fig. 5, experimental results on unrejoined DSBs per Gy as a function of repair time (20) are compared with calculations for the four scenarios in Table 3. Time constants due to parameter adaptation are also listed for joining of clean DNA ends as well as for cleaning of single-strand breaks and of relevant base lesions at dirty DNA ends. The initial reduction of DSBs in the first 20 min is reproduced in all scenarios; it is closely related to the joining of clean DNA ends in the postsynaptic phase as the rate-limiting step of the calculation. Later, after 30 to about 90 min, scenarios B and C have higher yields of unrejoined DSBs than the experimental results and the fitted curve, whereas scenario D deviates in particular due to lower rejoining activity after 3 h repair time. Scenario A shows the best agreement with the experimental data and their fit curve.

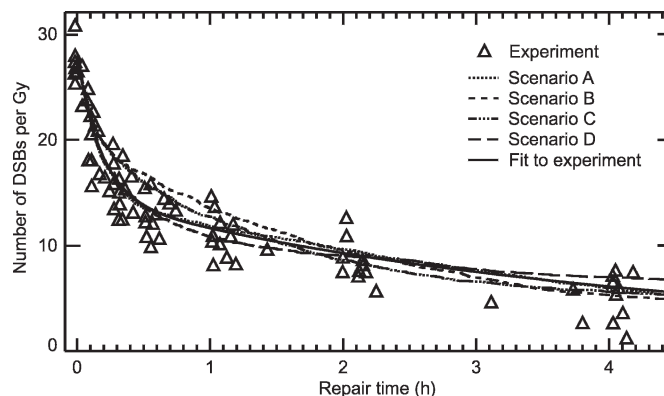


FIG. 5. Calculated rejoining of DSBs in human fibroblast cell lines after exposure to 40 Gy ¹³⁷Cs γ rays compared to experimental data (20) with low temperature lysis.

TABLE 3
Assumptions and Parameters for Simulated Scenarios

Scenario	A	B	C	D
Diffusive motion during presynaptic phase initially after DSB induction	low	high	high	low
Diffusion coefficient	1 nm ² /s	100 nm ² /s	100 nm ² /s	1 nm ² /s
Diffusive motion later in presynaptic phase	low	high	high	high
Diffusion coefficient	1 nm ² /s	100 nm ² /s	100 nm ² /s	100 nm ² /s
Kinetics of clean and dirty DNA ends in presynaptic phase	identical	identical	different	identical
Parameter set in Table 2	K	K	M	K
Loss of synapsis in postsynaptic phase	no	no	no	yes
Time constant	— ^a	— ^a	— ^a	900 s
Time constant for cleaning of dirty DNA ends (step-by-step)	7800 s	3600 s	1800 s	600 s
Time constant for joining of clean DNA ends (single step)	1200 s	500 s	450 s	960 s

^a Not defined.

Fractions of DNA Ends in Presynaptic and Postsynaptic States

In Fig. 6, calculated fractions of DSBs in presynaptic states and in postsynaptic (but not joined) states are plotted in panel A and panel B, respectively, as a

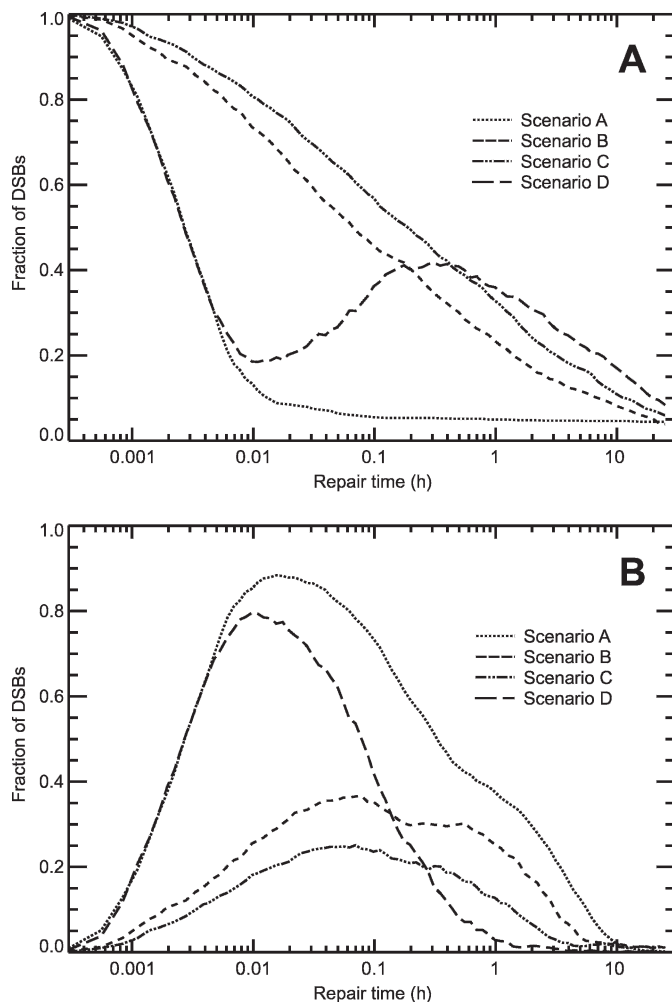


FIG. 6. Calculated fraction of DNA ends in presynaptic states (panel A) and in postsynaptic states (panel B) after exposure to 40 Gy ¹³⁷Cs γ rays.

function of repair time. In scenarios A and D, low and initially low diffusion results in fast reduction of the presynaptic fraction, respectively. In scenario A the presynaptic fraction decreases below 10% in less than 1 min but then stays almost constant. Due to dissociative processes in the postsynaptic phase, the presynaptic fraction in scenario D rises again after half a minute and reaches another maximum at about 20 min repair time. Scenarios B and C show a continuous decrease of their relatively high values over the whole time span; presynaptic fractions exceed the postsynaptic fractions (panel B) except for scenario B in the interval from 0.5 to 3 h. High fractions in postsynaptic states are found for scenarios A and D after 1 min. In all scenarios the fraction of DNA ends in postsynaptic states is rather small after some hours; the majority of unrejoined DNA ends is then in presynaptic states.

Fraction of Misrejoined DSBs

Calculated fractions of incorrectly rejoining (including unrejoined) DSBs after 80 Gy γ -ray exposure are plotted in Fig. 7 as a function of repair time together with corresponding experimental results (33) for primary lung fibroblasts and dermal fibroblasts after 80 Gy X irradiation. In scenario A, this fraction decreases from 0.45 to 0.08 between 1 and 12 h repair time, whereas it decreases to fractions between 0.4 and 0.48 after 12 h in scenarios B, C and D, in overall agreement with the experimental results (33). In ref. (33), the data were fitted by a long-term value of 0.51 approached exponentially with a time constant of 0.38 h; in scenarios C and D, the final value is reached with similar kinetics.

Dose-Dependent Yields of Residual DSBs, Misrejoined DSBs and Chromosomal Aberrations

During the first few hours of repair, the calculated time course of DSB rejoining has only a minor dependence on dose (data not shown). However, after longer repair times, the calculated fractions of residual

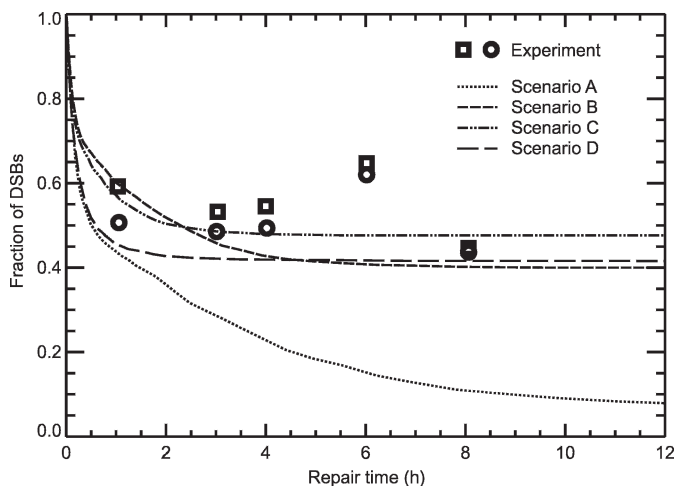


FIG. 7. Calculated fraction of incorrectly rejoined DSBs after exposure to 80 Gy ^{137}Cs γ rays compared with experimental data (33) for primary lung (circles) and dermal (squares) fibroblasts after exposure to 80 Gy 80 kV X rays.

DSBs tend to increase with decreasing dose in scenarios B, C and D. Figure 8 shows the calculated dose-dependent yields of residual DSBs after 24 h of repair time. For scenario A, this yield increases almost linearly with increasing dose, corresponding to a dose-independent fraction of about 5%. For scenarios B, C and D, the steep initial rise declines above about 20 Gy to a reduced linear increase with a tendency to saturate at the highest calculated dose value, corresponding to a decrease of the fraction of residual DSBs from 15–25% at 1 Gy to 3–5% at 80 Gy. The experimental data, however, have a different dose dependence, as shown in Fig. 8. The yields of residual DSBs can usually be fitted adequately by linear-quadratic functions with a more or

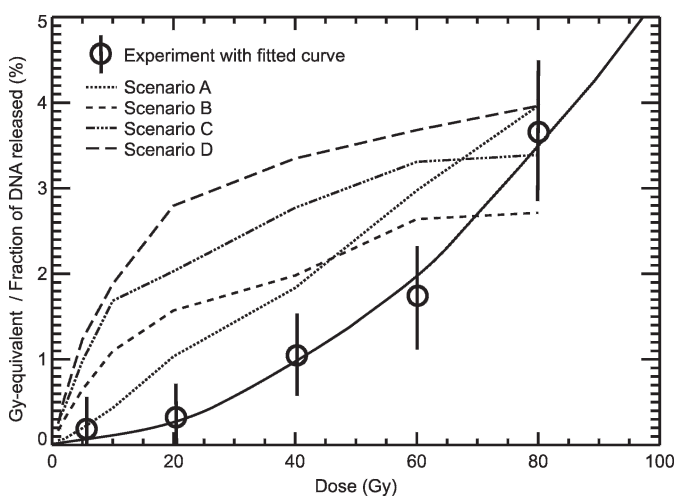


FIG. 8. Calculated dose-dependent yield of residual DSBs due to ^{137}Cs γ rays after 24 h repair time, presented as Gy-equivalent to initial DSB induction, compared with the dose-dependent yield of residual DSBs due to 200 kVp X rays after 24 h repair time, presented as the fraction of DNA released from a typical skin fibroblast cell line using a constant-field gel electrophoresis protocol, and a linear-quadratic fit to these experimental data (35).

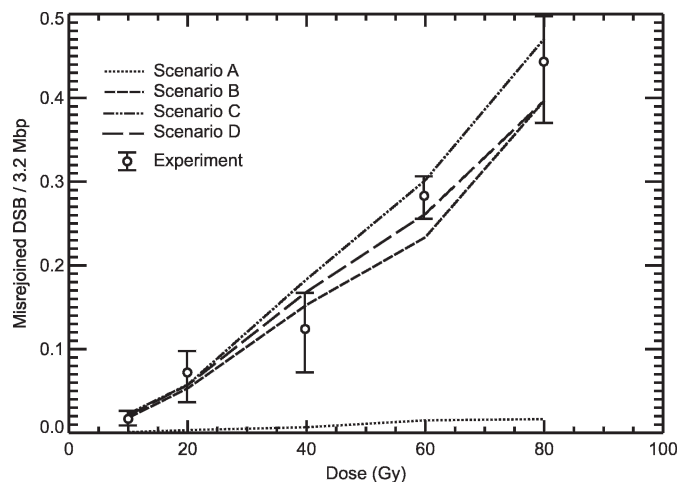


FIG. 9. Calculated yield of misrejoined DSBs per 3.2-Mbp genomic length induced by ^{137}Cs γ rays compared to experimental misrejoining yields induced by 320 kVp X rays on a 3.2-Mbp DNA fragment (37).

less pronounced quadratic term (34–36); thus the fractions of residual DSBs depend linearly on dose with a higher or smaller gradient. The absolute values of residual DSBs depend strongly on the cell system and the experimental protocol. In ref. (37), nonrejoined breaks at 16 h after X irradiation were less than 2% of the DSBs originally formed.

In Fig. 9, calculated yields of misrejoined DSBs, normalized to a genomic length of 3.2 Mbp, are plotted together with experimental yields of misrejoined DSBs on a 3.2-Mbp DNA fragment after exposure to 320 kVp X rays (37). Scenarios B, C and D are in good agreement with the experimental data, whereas the result of scenario A is too low by a factor of about 20.

In Fig. 10, the calculated numbers of misrejoining events involving different chromosomes are presented as a function of dose together with experimental results

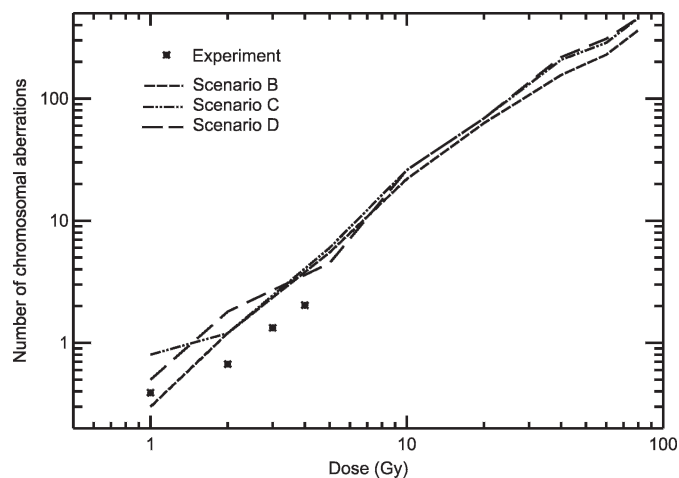


FIG. 10. Calculated numbers of chromosomal aberrations as a function of exposure to ^{137}Cs γ rays compared with experimental results after exposure to 250 kV X rays (38).

(38) for the induction of chromosomal aberrations. In scenario A, only one such event was obtained in a calculation for 40 Gy. The experimental data tend to be lower than the calculated numbers for scenarios B, C and D; however, the deviation is not more than a factor of 3, and the dose dependence is reproduced fairly well.

DISCUSSION

The present work is the first approach that combines track structure-based information on initial radiation damage on a molecular level, its spatial distribution within the cell nucleus, its spreading along the genome, and information on elementary processes of DNA repair aimed at calculating the time course of DSB rejoining with a subdivision into the four end points correct rejoining, chromosomal aberration induction, other misrejoining events, and fractions of residual DSBs. It extends the temporal dimension of our biophysical model PARTRAC, ending with initial radiation damage simulation after less than a microsecond, by about 13 orders of magnitude up to the end of DNA repair processes after a few days. In its present structure, the repair model is far from being mature; however, the methodology is capable of offering a wide field for model improvements.

The presynaptic phase of the present model refers to molecular events of the DNA-PK dependent NHEJ pathway; other routes to joining of DNA ends, in particular those of the B-NHEJ pathways (39), have not been taken into account. Such alternative pathways can be readily included in the model provided that a quantitative description of essential steps of the process and its interrelationship with the usual NHEJ pathway has been established. Shortcomings of present model calculations, in particular in later stages of the repair process, may result more or less from alternative repair pathways that have not been considered in the simulation; however, in the following discussion, the influence of other pathways on the end points considered is disregarded.

Another topic that needs further consideration is the initial condition for the DNA repair model. In the present work, the initial radiation damage calculation in PARTRAC has been reassessed in view of experimental results demonstrating that heat-labile sites that appear as DSBs under experimental protocols with a warm lysis step make up a greater fraction of measured DSBs. Reasonable yields after γ irradiation have been calculated by assigning OH radical interactions with sugar into almost equal fractions leading to prompt strand breaks, heat-labile sites and neither of these end points. It was shown recently (40) that most heat-labile sites form DSBs not only at elevated lysis temperature (50°C) but also at physiological temperature (37°C); thus

additional transformation of heat-labile sites to DSBs during the initial phase of the repair process may be needed in future calculations.

The present characterization of base lesions is given by the energy deposition events and the number of OH radical interactions. About 56% of the DNA ends include such base lesions, and about 62% of the DSBs are complex if all nearby base lesions and single-strand breaks at both sides of the DSB are considered; this fraction agrees with the modeling result in ref. (23). Assuming that all these base lesions delay DNA repair leads to rather small fast rejoining fraction of about 20%, which conflicts with experimental results (20) and precludes concordant repair kinetics. The adopted subset of relevant base lesions reduces the fraction of complex DSBs and dirty DNA ends to 48% and 37%, respectively, and allows consistency in repair kinetics between the model and the experiment. Heat-labile sites have not been considered as lesions that contribute to dirty DNA ends. Refined characterization of base damage may improve the agreement between the experiment and the calculation; it may even be essential for reasonable calculations of DNA repair after high-LET irradiation.

Not yet included in the model is the formation of foci that apparently occur during DNA repair a certain time after DSB induction and disappear later when the process is supposed to be finished. To include this end point in our model, the conditions for the formation and destruction of foci have to be determined in relation to the interaction scheme. This was beyond the scope of the present work; however, it will be helpful to compare experimental results on focus formation directly with corresponding calculations in the future.

Simulation calculations for the presynaptic phase demonstrate that the time constants are not uniquely identifiable from adaptation to measured recruitment of Ku80 and DNA-PK. The time constants adopted for these recruitment processes based on measured repair enzyme attachment to DNA termini (27, 28) are about 50-fold longer than those derived from reaction kinetics data; reaction constants of $7-8 \times 10^6 M^{-1} s^{-1}$ and $1.4 \times 10^8 M^{-1} s^{-1}$ (28) multiplied by concentrations of $2 \mu M$ and $0.4 \mu M$ (3) yield time constants of 0.07 s and 0.02 s for attachment of Ku70/Ku80 and DNA-PKcs to DNA termini, respectively. This difference may result partly from chromatin remodeling processes that first have to make the DNA termini accessible to the Ku heterodimer and DNA-PKcs and partly from a generally slower kinetics within the nuclear environment compared to the experimental system in ref. (28). The presynaptic phase affects the DNA repair process essentially via the time course by which DNA ends enter synapsis. This is determined in the present model by the mobility of DNA ends, i.e., how fast complementary DNA ends lose their proximity.

The scenarios of simulation calculations A, B, C and D correspond to different simplified working hypotheses about the origin of slow repair during the later period of the biphasic time course of DSB rejoining: (A) the slow cleaning of dirty DNA ends after almost complete early synapsis, (B) the loss of vicinity of complementary DNA ends leads to frequent missing of early synapsis before DNA-PK attachment, (C) the frequent missing of early synapsis for dirty DNA ends only, and (D) the frequent break-up of the synaptic repair complex and the restart of the repair process. In scenarios B, C and D, cleaning of dirty DNA ends also contributes to delayed repair. For each of these scenarios, a reasonable adaptation of calculated unrejoined DSBs to corresponding experimental data (20) has been achieved with an initial fast phase followed by a phase of slower repair. The initial fast phase is related mainly to the joining of clean DNA ends after the early synapsis of formerly linked DNA ends. A single rate-limiting step in the subsequent joining procedure corresponds to an initially exponential decrease; reduced fractions of DNA ends entering early synapsis in scenarios B and C are compensated by a reduced time constant. Modeling this fast joining of clean DNA ends as a step-by-step process corresponding to the number of base pairs of the overhang length yielded a subdivision of the fast repair phase into an initial stage of about 3 min with enhanced repair rate and subsequent slower rejoining. Since experimental results do not support such a behavior, fast joining has been described as a single-step process that is independent of overhang length. Cleaning of dirty DNA ends may also be considered as a single process with a unique time constant that is independent of the number of lesions. Corresponding calculations gave results similar to the usual step-by-step process for each lesion with an increased time constant. For strand breaks and relevant base lesions, the same time constant has been used because a solid adaptation of two time constants based on data for low-LET radiation is not feasible. For this task, data for high-LET radiation will have to be considered.

The bi-exponential curve fitted to the experimental data (20) is almost perfectly reproduced by scenario A. This is not surprising since the model has a single rate-limiting step for the repair of clean DNA ends, and the majority of dirty DNA ends need a single cleaning step. Early synapsis of more than 90% of the DNA ends reduces the relevance of spatial characteristics to a minor factor according to the small complementary fraction of DNA ends that have missed early synapsis. Low diffusion of the residual DNA ends leads to minimal joining activity in the long term. These characteristics of scenario A result, unlike the other scenarios, in small and dose-independent fractions of incorrectly joined DSBs, small yields of misrejoined DSBs, and almost no chromosomal aberrations. Dis-

crepancies with experimental results for misrejoining and chromosomal aberration induction highlight that the spatial dimension is a key element in the DSB repair process. In scenarios B, C and D, the time course of DSB rejoining deviates from the bi-exponential curve and also partly from experimental results in some intervals, but the fractions of incorrectly rejoined DSBs as well as the dose-dependent yields of misrejoined DSBs and of chromosomal aberrations are in unanticipated agreement with experimental results without any adaptation. No scenario is obviously superior to the others. The high degree of agreement for misrejoining events and chromosomal aberration induction, even in its dependence on dose, highlights the interaction between the spatial and temporal aspects of DNA repair since movement of DNA ends is essential for its production, whereas parameter adaptation in the calculations was restricted to temporal characteristics. The restriction of movement around nuclear attachment sites and their distribution within the DNA target model are important factors for the ratio between intrachromosomal misrejoining and chromosomal aberration induction. In all comparisons with experimental results, it should be kept in mind that the experimental limitations in resolution of short DNA fragments may significantly bias the results (41). In the present analysis we did not consider whether misrejoined DSBs or chromosomal aberrations would be detectable in corresponding experiments.

The calculated dose-dependent residual DSBs after 1 day illustrate the deficiencies of the present version of the DNA repair model. Movement of free DNA ends according to Brownian motion in a homogeneous liquid combined with an interaction distance of molecular size for synapsis of two DNA ends is obviously an approach that needs improvement. In particular, after low radiation doses and correspondingly small numbers of initial DSBs, the number of encounter events of free DNA ends is too small to maintain sufficient repair activity to eventually rejoin almost all DNA ends. The late phase of DSB rejoining apparently is not a diffusion-controlled interaction process of free DNA ends, although it may be appropriate during earlier phases of the process after higher radiation doses.

Refined assumptions on the interaction and motion of DNA ends will need to be developed and tested to reproduce the low, almost constant or, with increasing dose, slightly rising fraction of unrejoined DSBs found in experimental data (34, 35). This requires a spatio-temporal setup of the model that keeps or brings all DNA ends in proximity and interaction that is largely independent of their number without reduction of the pathways toward misrejoining and chromosomal aberration induction. Residual DSBs after long repair times may also be attributed to new mechanisms like blocked cleaning of dirty DNA ends for certain patterns of nearby lesions. Such an approach will have to be

tested in particular in view of experimental results after high-LET irradiation. The present methodology is capable of corresponding improvements of the DNA repair model.

CONCLUSION

The present model of DNA DSB repair via NHEJ is a suitable framework for a mechanistic representation of basic processes occurring in cell nuclei in response to radiation-induced DSB induction. Comprehensive data from the biophysical model PARTRAC about initial DNA damage concerning the local structure of damage clusters and lesion distribution within the cell nucleus, on the genome and in relation to nuclear attachment sites are taken into account in the repair model to predict the system behavior over a time up to days after the radiation insult. First application of the model to repair processes in human fibroblast cells after low-LET irradiation reproduced rejoining kinetics, yields of misrejoining events, and chromosomal aberration induction; however, model improvements are needed in view of the residual DSBs after low radiation doses. Forthcoming investigations will consider a variety of radiation qualities to improve the assignment of differences in initial damage to dynamics and results of DNA repair processes. The present results stimulate further efforts toward this challenging undertaking.

ACKNOWLEDGMENT

This work was partially supported by the EC within the framework of the project 'RISC-RAD' (FI6R-CT.2003-508842).

Received: August 6, 2009; accepted: November 30, 2009; published online: March 1, 2010

REFERENCES

1. S. P. Lees-Miller and K. Meek, Repair of DNA double strand breaks by non-homologous end joining. *Biochimie* **85**, 1161–1173 (2003).
2. E. Weterings and D. J. Chen, The endless tale of non-homologous end-joining. *Cell Res.* **18**, 114–124 (2008).
3. M. R. Lieber, Y. Ma, U. Pannicke and K. Schwarz, Mechanism and regulation of human non-homologous DNA end-joining. *Nat. Rev. Mol. Cell Biol.* **4**, 712–720 (2003).
4. D. C. van Gent and M. van der Burg, Non-homologous end-joining, a sticky affair. *Oncogene* **26**, 7731–7740 (2007).
5. S. B. Curtis, Lethal and potentially lethal lesions induced by radiation – a unified repair model. *Radiat. Res.* **106**, 252–270 (1986).
6. R. D. Stewart, Two-lesion kinetic model of double-strand break rejoining and cell killing. *Radiat. Res.* **156**, 365–378 (2001).
7. F. A. Cucinotta, H. Nikjoo, P. O'Neill and D. T. Goodhead, Kinetics of DSB rejoining and formation of simple chromosome exchange aberrations. *Int. J. Radiat. Biol.* **76**, 1463–1474 (2000).
8. W. R. Holley, I. S. Mian, S. J. Park, B. Rydberg and A. Chatterjee, A model for interphase chromosomes and evaluation of radiation-induced aberrations. *Radiat. Res.* **158**, 568–580 (2002).
9. P. Hahnfeldt and L. R. Hlatky, A Monte Carlo/Markov chain model for the association of data for chromosome aberrations and formation of micronuclei. *Radiat. Res.* **138**, 239–245 (1994).
10. M. Pinto, K. M. Prise and B. D. Michael, A Monte Carlo model of DNA double-strand break clustering and rejoining kinetics for the analysis of pulsed-field gel electrophoresis data. *Radiat. Res.* **162**, 453–463 (2004).
11. M. Pinto, K. M. Prise and B. D. Michael, Evidence for complexity at the nanometer scale of radiation-induced DNA DSBs as a determinant of rejoining kinetics. *Radiat. Res.* **164**, 73–85 (2005).
12. F. A. Cucinotta, J. M. Pluth, J. A. Anderson, J. V. Harper and P. O'Neill, Biochemical kinetics model of DSB repair and induction of gamma-H2AX foci by non-homologous end joining. *Radiat. Res.* **169**, 214–222 (2008).
13. W. Friedland, H. G. Paretzke, F. Ballarini, A. Ottolenghi, G. Kreth and C. Cremer, First steps towards systems radiation biology studies concerned with DNA and chromosome structure within living cells. *Radiat. Environ. Biophys.* **47**, 49–61 (2008).
14. W. Friedland, P. Jacob, P. Bernhardt, H. G. Paretzke and M. Dingfelder, Simulation of DNA damage after proton irradiation. *Radiat. Res.* **159**, 401–410 (2003).
15. D. E. Cullen, J. H. Hubbel and L. Kissel, *EPDL97 The evaluated data library, '97 version*. Lawrence Livermore National Laboratory, 1997.
16. M. Dingfelder, D. Hantke, M. Inokuti and H. G. Paretzke, Electron inelastic-scattering cross sections in liquid water. *Radiat. Phys. Chem.* **53**, 1–18 (1998).
17. M. Dingfelder, R. H. Ritchie, J. E. Turner, W. Friedland, H. G. Paretzke and R. N. Hamm, Comparisons of calculations with PARTRAC and NOREC: transport of electrons in liquid water. *Radiat. Res.* **169**, 584–594 (2008).
18. M. S. Kreipl, W. Friedland and H. G. Paretzke, Time- and space-resolved Monte Carlo study of water radiolysis for photon, electron and ion irradiation. *Radiat. Environ. Biophys.* **48**, 11–20 (2009).
19. G. Kreth, S. K. Pazhanisamy, M. Hausmann and C. Cremer, Cell type-specific quantitative predictions of radiation-induced chromosome aberrations: a computer model approach. *Radiat. Res.* **167**, 515–525 (2007).
20. K. H. Karlsson, I. Radulescu, B. Rydberg and B. Stenerlow, Repair of radiation-induced heat-labile sites is independent of DNA-PKcs, XRCC1 and PARP. *Radiat. Res.* **169**, 506–512 (2008).
21. P. Bernhardt, W. Friedland, P. Jacob and H. G. Paretzke, Modeling of ultrasoft X-ray induced DNA damage using structured higher order DNA targets. *Int. J. Mass Spectrom.* **223–224**, 579–597 (2003).
22. M. S. Kreipl, W. Friedland and H. G. Paretzke, Interaction of ion tracks in spatial and temporal proximity. *Radiat. Environ. Biophys.* **48**, 349–359 (2009).
23. H. Nikjoo, P. O'Neill, W. E. Wilson and D. T. Goodhead, Computational approach for determining the spectrum of DNA damage induced by ionizing radiation. *Radiat. Res.* **156**, 577–583 (2001).
24. B. Jakob, J. Splinter, M. Durante and G. Taucher-Scholz, Live cell microscopy analysis of radiation-induced DNA double-strand break motion. *Proc. Natl. Acad. Sci. USA* **106**, 3172–3177 (2009).
25. G. L. Lukasc, P. Haggie, O. Seksek, D. Lechardeur, N. Freedman and A. S. Verkman, Size-dependent DNA mobility in cytoplasm and nucleus. *J. Biol. Chem.* **275**, 1625–1629 (2000).
26. M. J. Kruhlak, A. Celeste and A. Nussenzweig, Spatio-temporal dynamics of chromatin containing DNA breaks. *Cell Cycle* **5**, 1910–1912 (2006).

27. N. Uematsu, E. Weterings, K. Yano, K. Morotomi-Yano, B. Jakob, G. Taucher-Scholz, P. O. Mari, D. C. van Gent, B. P. Chen and D. J. Chen, Autophosphorylation of DNA-PKcs regulates its dynamics at DNA double-strand breaks. *J. Cell Biol.* **177**, 219–229 (2007).
28. A. Taghva, Y. Ma and M. R. Lieber, Analysis of the kinetic and equilibrium binding of Ku protein to DNA. *J. Theor. Biol.* **214**, 85–97 (2002).
29. R. B. West, M. Yaneva and M. R. Lieber, Productive and nonproductive complexes of Ku and DNA-dependent protein kinase at DNA termini. *Mol. Cell Biol.* **18**, 5908–5920 (1998).
30. P. O. Mari, B. I. Florea, S. P. Persengiev, N. S. Verkaik, H. T. Bruggenwirth, M. Modesti, G. Giglia-Mari, K. Bezstarosti, J. A. Demmers and D. C. van Gent, Dynamic assembly of end-joining complexes requires interaction between Ku70/80 and XRCC4. *Proc. Natl. Acad. Sci. USA* **103**, 18597–18602 (2006).
31. L. Spagnolo, A. Rivera-Calzada, L. H. Pearl and O. Llorca, Three-dimensional structure of the human DNA-PKcs/Ku70/Ku80 complex assembled on DNA and its implications for DNA DSB repair. *Mol. Cell* **22**, 511–519 (2006).
32. P. Y. Wu, P. Frit, L. Malivert, P. Revy, D. Biard, B. Salles and P. Calsou, Interplay between Cernunnos-XLF and nonhomologous end-joining proteins at DNA ends in the cell. *J. Biol. Chem.* **282**, 31937–31943 (2007).
33. M. Lobrich, M. Kuhne, J. Wetzel and K. Rothkamm, Joining of correct and incorrect DNA double-strand break ends in normal human and ataxia telangiectasia fibroblasts. *Genes Chromosomes Cancer* **27**, 59–68 (2000).
34. B. Stenerlow, E. Blomquist, E. Grusell, T. Hartman and J. Carlsson, Rejoining of DNA double-strand breaks induced by accelerated nitrogen ions. *Int. J. Radiat. Biol.* **70**, 413–420 (1996).
35. E. Dikomey, I. Brammer, J. Johansen, S. M. Bentzen and J. Overgaard, Relationship between DNA double-strand breaks, cell killing, and fibrosis studied in confluent skin fibroblasts derived from breast cancer patients. *Int. J. Radiat. Oncol. Biol. Phys.* **46**, 481–490 (2000).
36. J. Dahm-Daphi and E. Dikomey, Non-reparable DNA strand breaks and cell killing studied in CHO cells after X-irradiation at different passage numbers. *Int. J. Radiat. Biol.* **66**, 553–555 (1994).
37. B. Rydberg, B. Cooper, P. K. Cooper, W. R. Holley and A. Chatterjee, Dose-dependent misrejoining of radiation-induced DNA double-strand breaks in human fibroblasts: experimental and theoretical study for high- and low-LET radiation. *Radiat. Res.* **163**, 526–534 (2005).
38. E. Nasonova, K. Fussel, S. Berger, E. Gudowska-Nowak and S. Ritter, Cell cycle arrest and aberration yield in normal human fibroblasts. I. Effects of X-rays and 195 MeV u⁻¹ C ions. *Int. J. Radiat. Biol.* **80**, 621–634 (2004).
39. G. Iliakis, H. Wang, A. R. Perrault, W. Boecker, B. Rosidi, F. Windhofer, W. Wu, J. Guan, G. Terzoudi and G. Pantelias, Mechanisms of DNA double strand break repair and chromosome aberration formation. *Cytogenet. Genome Res.* **104**, 14–20 (2004).
40. S. K. Singh, W. Wu, M. Wang and G. Iliakis, Extensive repair of DNA double-strand breaks in cells deficient in the DNA-PK-dependent pathway of NHEJ after exclusion of heat-labile sites. *Radiat. Res.* **172**, 152–164 (2009).
41. A. Campa, D. Alloni, F. Antonelli, F. Ballarini, M. Belli, V. Dini, G. Esposito, A. Facchetti, W. Friedland and M. A. Tabocchini, DNA fragmentation induced in human fibroblasts by ⁵⁶Fe ions: experimental data and Monte Carlo simulations. *Radiat. Res.* **171**, 438–445 (2009).